MATERIALS PHYSICS AND MECHANICS RESEARCH ARTICLE

Submitted: August 23, 2023 **Revised: November 28, 2025** **Accepted: December 8, 2025**

Computational study of Ba-doped TiO_3 perovskites for solar energy applications

A. Kumar [1], R. Srivastava [2], A. Kumar [3], R. Kumar [4], S. Kumar [5], R. Chand [6], D. Saxena [7], A. Kumar [8] ✉

[1] Department of Physics, Mahamaya Government Degree College, Sherkot, Bijnor, Uttar Pradesh, India

[2] Department of Education Utkal Mani Gopabandhu Das, Faculty of Education, Swami Vivekananda, Subharti University, Meerut, UP, India

[3] Electrical Engineering, Subharti Polytechnic College, Swami Vivekanand, Subharti University, Meerut, UP, India

[4] Department of Mathematics, KVSCOS, Swami Vivekanand, Subharti University, Meerut, UP, India

[5] Department of Physics, SRM Institute of Science and Technology, Delhi NCR Campus Modinagar, UP, India

[6] Department of Applied Sciences (Physics), Meerut Institute of Engineering and Technology, Meerut Uttar Pradesh, India

[7] Department of Physics, Ismail National Mahila PG College, Meerut Uttar Pradesh, India

[8] Department of Physics, KVSCOS, Swami Vivekanand, Subharti University, Subhartipuram Meerut, India

✉ 01amankumar@gmail.com

ABSTRACT

The remarkable electrical and optical properties of barium doped TiO_3 perovskite make it an appealing material for optoelectronic applications. This study comprehensively investigates the structural, electrical, and optical characteristics of $BaTiO_3$ using density functional theory. The electrical characteristics, such as the energy band structure and density of states, were carefully examined. A band gap of 1.92 eV was discovered by the TB-mBJ functional, which is in good agreement with earlier experimental and theoretical findings. The partial density of states analysis reveals that the Ba-p, Ti-d, and O-p states have a significant impact on the material's electronic structure. By evaluating critical variables, the optical properties of $BaTiO_3$ were investigated. The TB-mBJ approximation indicates that the optical spectrum reveals $BaTiO_3$ has remarkable properties in the 4–5 eV energy range, making it suitable for solar energy harvesting. Its potential for integration into perovskite solar cells and other optoelectronic devices requiring high optical sensitivity is further corroborated by its low reflectance in this spectrum.

KEYWORDS

perovskite material • TB-mBJ • WIEN2K • GGA • density functional theory

Citation: Kumar A, Srivastava R, Kumar A, Kumar R, Kumar S, Chand R, Saxena D, Kumar A. Computational study of Ba-doped TiO_3 perovskites for solar energy applications. *Materials Physics and Mechanics.* 2025;54(6): 53–62. http://dx.doi.org/10.18149/MPM.5362025_5

Introduction

The chemical formula ABX_3, where A and B denote cations and X signifies an anion, characterizes perovskite materials. The materials in question demonstrate remarkable suitability for solar energy applications, attributed to their outstanding optoelectronic characteristics. These include a long carrier diffusion length, low trap state density, high

absorption coefficient, excellent intrinsic carrier mobility, and an appropriate band gap [1–3]. This development may result in solar cells that are more effective, greatly increasing energy conversion rates. In the near future, researchers hope that these developments will open the door to sustainable energy solutions. Increase their potential for photovoltaic applications by producing photovoltages higher than their band gap. ABO3 perovskites' optical and electronic characteristics can be tuned through cationic substitution at either the A or B site, providing a great deal of design flexibility for functional materials [4–7]. Among these, barium titanate ($BaTiO_3$), which crystallizes in the ABO_3 perovskite structure and experiences a tetragonal phase transition at about 120 ºC, is a classic ferroelectric material [8–10]. $BaTiO_3$ is a topic of theoretical and experimental interest due to its exceptional ferroelectricity, piezoelectricity, pyroelectricity, high dielectric constant, wide bandgap, and low electrical loss [11,12]. Moreover, it has exceptional chemical and mechanical stability over an extensive temperature range. This stability makes it an ideal candidate for various industrial applications, including aerospace and automotive sectors, where materials are often exposed to harsh conditions. Additionally, its resistance to corrosion further enhances its suitability for long-term use in demanding environments. Owing to these properties, $BaTiO_3$ finds applications in sensors, actuators, waveguides, high-performance computing, laser frequency doubling, nanoelectronics, and aerospace technologies [13]. The phase transitions of $BaTiO_3$ exhibit significant temperature dependence. At 120 ºC, the material changes from a cubic phase (*Pm3m*) to a tetragonal phase (*P4mm*). At 5 ºC finally, at around -90 ºC, it changes to a rhombohedral phase (*R3m*) [14,15]. These phase transitions are crucial for understanding the material's properties and potential applications, particularly in the fields of electronics and materials science. The ability to manipulate the phases by varying temperature allows for tailored performance in different environments. Structural modifications make $BaTiO_3$ highly suitable for various applications, for semiconductor applications in solar energy [16–20]. Enabling adjustments to its lattice structure [20]. Empirical studies have demonstrated that $BaTiO_3$ possesses a substantial bandgap of approximately 3.00 eV, which deviates from theoretical predictions [21,22]. To mitigate energy losses in photovoltaic applications, this structure ensures robust charge carrier mobility and an extended diffusion length. The lattice constants of cubic and tetragonal $BaTiO_3$ are estimated to be roughly 3.958 and 3.954 Å, respectively, based on theoretical simulations using the PBE-GGA. These values are crucial to understanding the material's phase transitions and structural features. This provides a platform for future research on the ferroelectric and piezoelectric properties of $BaTiO_3$ under various circumstances. The values are marginally lower than the experimental results, which span from 3.996 to 4.006 Å [11].

This study systematically investigates the electrical and optical properties of $BaTiO_3$ for prospective application in perovskite solar cells, employing density functional theory (DFT). The study seeks to evaluate its technological viability by examining critical aspects such as lattice constants (Å), electronic bandgaps (eV), and state density prior to structural optimisation. The The TB-mBJ potential is utilized to improve the precision of band structure calculations.

Materials and Methods

A first-principles analysis of $BaTiO_3$ was carried out [23,24]. The electronic structure of $BaTiO_3$ was better understood thanks to these computations, which also helped to clarify its phase transitions. The accuracy and dependability of the results were also confirmed by comparing them to experimental data. To improve computational accuracy, we used the TB-mBJ method to incorporate the exchange-correlation effects. mBJ potential, which is known for its exceptional accuracy and produces an approximate deviation of only 2 % in band structure estimations of perovskites and semiconductors [25,26]. High-resolution Brillouin zone sampling was used for structural and electronic characterization using a carefully optimized 7 × 7 × 7 k-point mesh, which was then further refined to a denser 10 × 10 × 10 k-grid for increased precision. The VESTA software was used for structural visualization and crystallographic analysis, allowing for a thorough depiction of the polyhedral framework inherent in perovskite lattice configurations [27–30].

Results and Discussion

Structure properties

The P4mm space group is used to describe the tetragonal perovskite structure in which the $BaTiO_3$ compound crystallizes. In this context, six oxygen anions (O^{2-}) coordinate the barium cation (Ba^{2+}) octahedrally, while the titanium cation (Ti^{4+}) coordinates twelve times. The basic skeletal network is formed by corner-sharing between the TiO_6 octahedra, as shown in Fig. 1. Furthermore, the titanium cation occupies a central position inside the octahedral units.

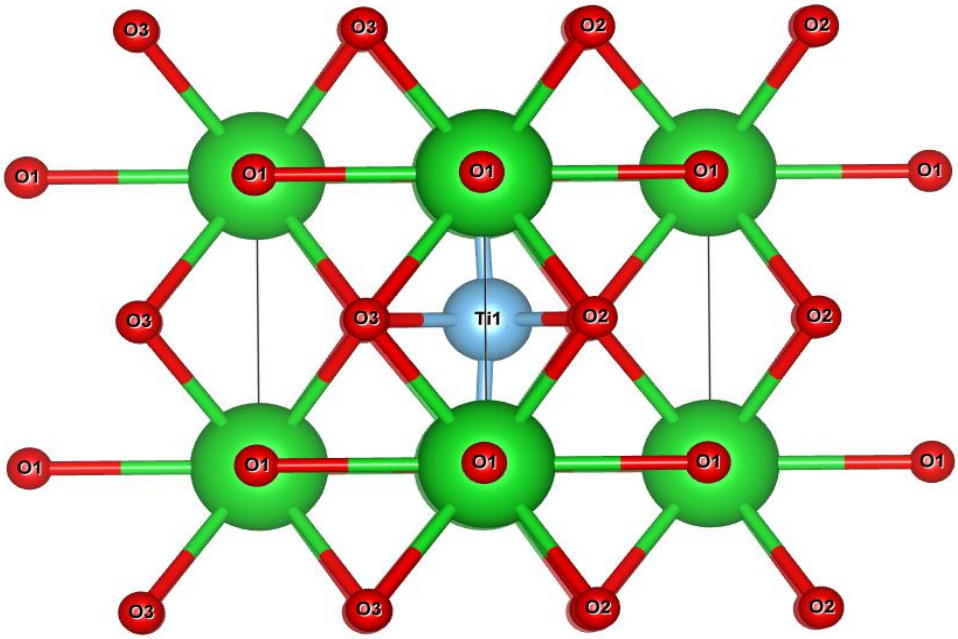

Fig. 1. Crystal structural of $BaTiO_3$ compound using VESTA simulation software

First-principles computing was used to improve the crystal structure and figure out the ground-state energy lattice parameters. The results showed that there was a strong

link between the lattice parameters and the physical properties of the material that were measured. The analysis also showed possible ways to improve the material's performance in a number of uses. The computed equilibrium lattice parameters, equilibrium volume and energy, bulk modulus, and first derivative for tetragonal $BaTiO_3$ are displayed in Table 1 and Fig. 2. These values are compared with existing experimental and theoretical datasets in a systematic way. The theoretical predictions match up very well with the reported experimental and computational results.

Table 1. Structural and electronic properties of $BaTiO_3$ compound using TB-mBJ approximation

Properties	$BaTiO_3$	Experimental
Lattice constant, Å	$a_0=b_0=4.068$	3.9988 [13]
	$c_0= 4.183$	4.0222 [13]
Space group	*P4mm* (99)	
Wyckoff position	Ba (0,0,0) Ti (0.5, 0.5, 0.5) O (0.5, 0.0, 0.48), (0.0, 0.5, 0.48) and (0.5, 0.5, 0.96)	
Minimum volume V_o, a.u^3	445.7012	
Minimum energy E_0, Ry	-18438.63743	
Bulk modulus B_0, GPa	159.3559	
First derivative of bulk modulus B_0', GPa	4.0942	
Band gap E_g, eV	1.92	1.56 [31,32]

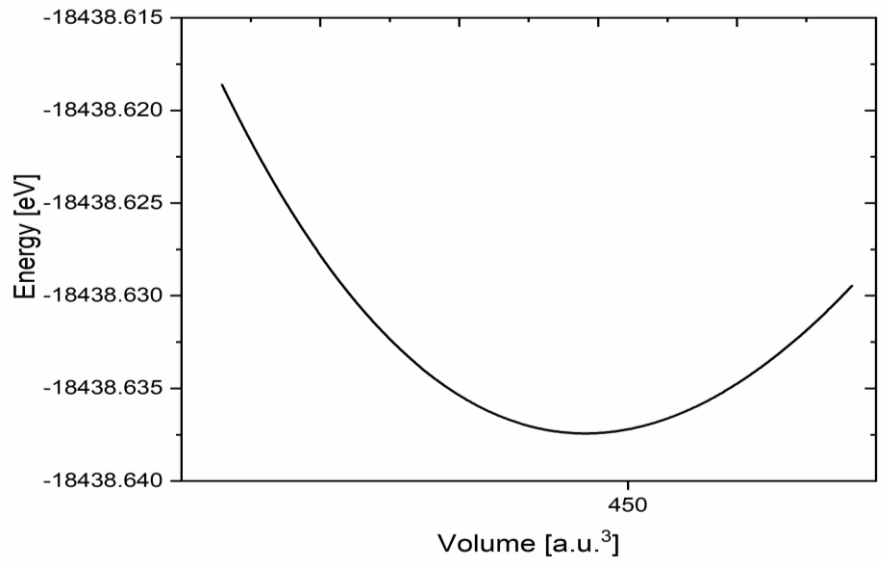

Fig. 2. Equilibrium volume V_s equilibrium energy curve of $BaTiO_3$ using Birch–Murnaghan equation of state (EOS) equation

Electronic properties

The electronic BS and DOS of $BaTiO_3$ have been investigated with help of TB-mBJ exchange potential [33–37]. The wave vector passes through high-symmetry points in the Brillouin zone along a particular k-point path. An estimate of the $BaTiO_3$ band structure is presented in Fig. 3. The Fermi energy located at origin. With the VBM point at the top and the CBM point at the bottom, the TB-mBJ approximation demonstrates that $BaTiO_3$ has an indirect

band gap. This method gives a band gap of 1.92 eV. This value matches what has been seen in experiments and $BaTiO_3$'s electronic properties, which are very important for using it in piezoelectric devices and ferroelectric materials. However, DFT calculations tend to underestimate the band gap because of the inherent problems with DFT-based methods, such as the fact that the energy derivative changes when the number of electrons changes. This underestimation happens because self-energy corrections and excited-state interactions are not handled well enough. The method used is correct. Figure 4 shows some important information that the study gives us.

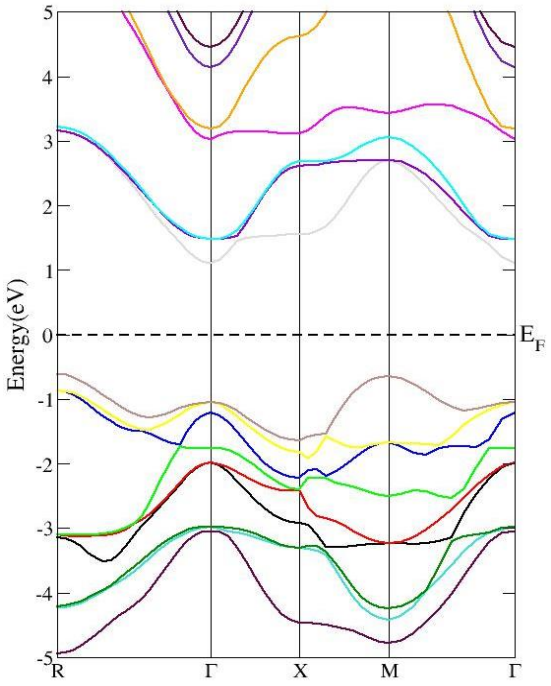

Fig. 3. Band structure of $BaTiO_3$

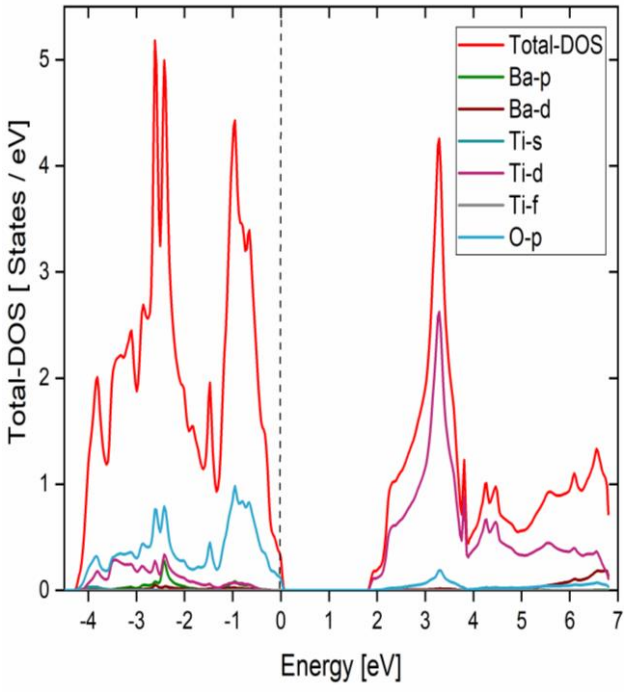

Fig. 4. Density of state of $BaTiO_3$

The impact of individual atomic orbitals on the DOS is displayed by the projected density of states (PDOS). According to the analysis, the titanium and oxygen orbitals make substantial contributions, especially in the valence band region. This realization aids in comprehending $BaTiO_3$ electrical characteristics and possible uses in piezoelectric devices. The unoccupied electronic states in this work have been analyzed using the PDOS, which takes into account contributions from the Ba-p, Ba-d, Ti-d, Ti-f, and O-p orbitals. 1.92 eV is found to be the calculated valence bandwidth for TB-mBJ in the tetragonal phase.

Optical properties

Figures 5(a–d) show the calculated optical properties of $BaTiO_3$. These elements include the optical conductivity σ(ω) shown in Fig. 5(b), the dielectric function $\varepsilon(\omega)$ shown in Fig. 5(a), the refractive index $n(\omega)$ shown in Fig. 5(c), and the reflectivity $R(\omega)$ shown in Fig. 5(d). Figure 5(a) shows the real and imaginary components of the dielectric functions with respect to the photon energy. The findings show that the optical responses of $BaTiO_3$ exhibit distinct behaviors across a range of energies. It is important to note

that the dielectric function's real part exhibits significant change that impacts both reflectivity and refractive index, whereas the peaks in the imaginary part are closely associated with absorption. For accurate optical property calculations to guarantee convergence, a dense and uniformly distributed k-point mesh is essential [38,39]. The dielectric function has two components: $\varepsilon_1(\omega)$, which represents the electronic polarization and structural features of the material's bands, and $\varepsilon_2(\omega)$, which accounts for all possible electronic transitions from the occupied state to the vacant state. These elements are essential for comprehending the interactions between materials and electromagnetic fields, especially in fields like photonics and optoelectronics.

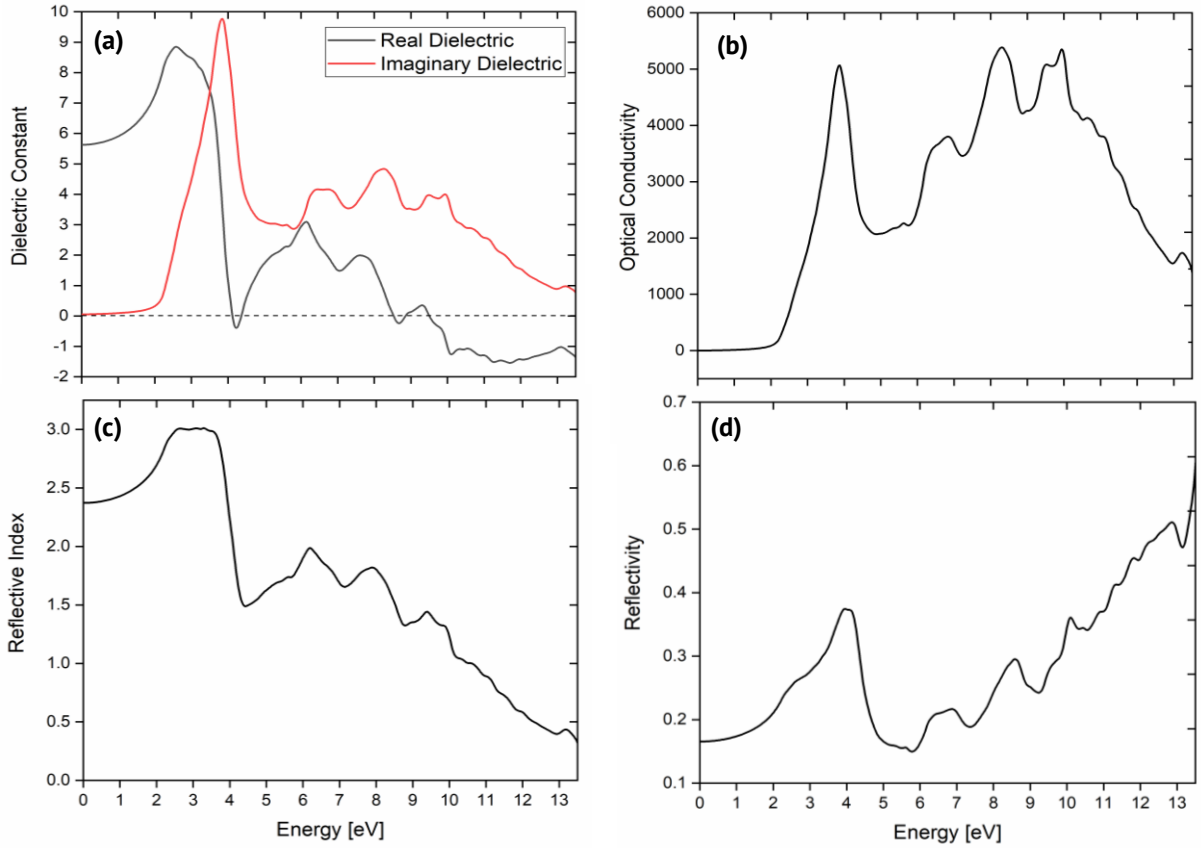

Fig. 5. Optical properties of (a) dielectric function $\varepsilon(\omega)$, (b) optical conductivity $\sigma(\omega)$, (c) refractive index $n(\omega)$, (d) reflectivity $R(\omega)$ for $BaTIO_3$

By examining the dielectric function, researchers can discover more about the optical characteristics and dynamics of various materials. This enables them to create increasingly sophisticated gadgets. $\varepsilon_1(0)$, in the TB-mBJ approximation is found to be 5.70. Moreover, $\varepsilon_1(\omega)$ shows negative values in the energy intervals of 4.0 and 9.50 to 13.5 eV, as shown in Fig. 5(a), suggesting the appearance of metallic properties in the UV spectrum. The relationship between energy dissipation from electronic transitions from the valence to the conduction band and the absorption spectrum is depicted in Fig. 5(a). Determine which orbitals are responsible for these changes by comparing the peaks in the $\varepsilon_2(\omega)$ curve with those in the DOS diagram in Fig. 4. It is possible to identify the electronic states that substantially influence the material's optical characteristics by examining these correlations. This knowledge is essential for customizing materials for

particular optoelectronic and photonic applications. The energy level at which $BaTiO_3$ exhibits optimal optical absorption and reduced polarization response is 3.90 eV, where $\varepsilon_2(\omega)$ reaches its maximum value based on the TB-mBJ approximation. Strong electronic transitions within the material are indicated by the distinct peaks in the optical conductivity $\sigma(\omega)$ of $BaTiO_3$. At photon energy of 8.5 eV, the optical conductivity reaches a maximum value of roughly 5500 $\Omega^{-1}cm^{-1}$, as illustrated in Fig. 5(b). Significant charge carrier excitation and energy dissipation mechanisms within this energy regime are suggested by the presence of such peaks. The optical transparency of $BaTiO_3$ is determined by its refractive index n(ω), which is directly related to its actual dielectric function, $\varepsilon_1(\omega)$, as shown in Fig. 5(c). The refractive index peaks at 2.4 at photon energies of 0 eV. $BaTiO_3$'s refractive index spectrum $n(\omega)$ exhibits two notable features.

The first is a noticeable peak that shows a strong optical response at about 3.0 eV. According to the Tb-mBJ approximation, the second is a region where the refractive index is less than unity and covers the photon energy range of 10.5 to 13.5 eV. Because of interactions with the electronic structure of the material, incident photons lose velocity when the refractive index rises above unity. This effect is further enhanced by a higher refractive index, which causes more. The first characteristic is a noticeable increase in the refractive index as the photon energy approaches the band gap. This indicates a stronger interaction between the material and light. The second characteristic is a distinct decrease in $n(\omega)$ with increasing energy level. This implies that as the material approaches the ultraviolet spectrum, its optical characteristics alter.

Generally speaking, any process that raises a material's electron density also raises its refractive index. The frequency-dependent optical reflectivity $R(\omega)$ of $BaTiO_3$, which is impacted by its complex dielectric functions, is displayed in Fig. 5(d). The amount of light that a substance reflects is known as its reflectivity. This property is essential for comprehending how the material behaves in a variety of applications, including electro-optic devices and capacitors. The changes in $R(\omega)$ disclose how various light frequencies interact with $BaTiO_3$'s dielectric characteristics, offering information about its possible applications in cutting-edge photonic technologies. It provides a comprehensive view of its light-responsiveness. Interestingly, under the Tb-mBJ approximation, $BaTiO_3$ shows noticeably increased reflectance.

The optical characteristics of $BaTiO_3$ demonstrate significant interaction with electromagnetic radiation, particularly within the UV-visible spectrum. The $\varepsilon_2(\omega)$ peak at 3.90 eV signifies pronounced interband transitions, corresponding to density of states contributions from O-2p to Ti-3d states. The refractive index $n(\omega)$ peaks at 2.4, showing strong light–matter interaction near the band edge, and decreases in the UV region. An abrupt increase in $\sigma(\omega)$ at around 8.5 eV indicates elevated optical conductivity resulting from excited carriers. The reflectivity $R(\omega)$ increases at elevated energies, indicating metallic characteristics. These findings illustrate the promise of $BaTiO_3$ in optoelectronic and photonic applications, particularly when using the TB-mBJ functional.

Conclusions

The structural, electronic, and optical characteristics of tetragonal $BaTiO_3$ are thoroughly examined in this first-principles investigation. The perovskite framework's stability is

confirmed by the optimized structural parameters, which also emphasize how important TiO_6 octahedral connectivity is to be preserving the crystal's integrity. These results support the potential of $BaTiO_3$ for use in ferroelectric and electronic devices. The indirect band gap of $BaTiO_3$ is 1.92 eV, according to electronic structure calculations performed with the TB-mBJ functional. Its use in sophisticated electronic and ferroelectric technologies is supported by the band structure and density of states (DOS) analyses, which provide important insights into its semiconducting behavior. To comprehend how the material interacted with electromagnetic radiation, the optical characteristics – such as the dielectric function, absorption coefficient, reflectivity, and refractive index – were assessed. In the ultraviolet region (4.0 and 9.5 – 13.5 eV), the real part of the dielectric function, $\varepsilon_1(\omega)$, exhibits negative values, signifying a shift toward metallic-like behavior. Strong optical absorption and electronic transitions are indicated by the imaginary part, $\varepsilon_2(\omega)$, peaking at 3.90 eV. A noticeable peak in the optical conductivity spectrum at 8.5 eV indicates strong interband transitions. With a notable peak at 3.0 eV, the refractive index exhibits a strong optical response, reaching a maximum value of 2.4 at 0 eV. It's interesting to note that the refractive index exhibits unusual dispersion behavior in the 10.5–13.5 eV range, falling below unity. The energy range where $\varepsilon_1(\omega)$ turns negative is represented by a clear peak in the reflectivity spectrum at 4.0 eV and a gradual increase beyond 5.0 eV. These findings confirm $BaTiO_3$ suitability for optoelectronic and photonic applications by highlighting the strong coupling between electronic transitions and optical responses.

CRediT authorship contribution statement

Anuj Kumar: writing – review & editing; **Ragini Srivastava**: supervision; **Amit Kumar**: data curation; **Rajiv Kumar**: data curation; **Sarvendra Kumar**: conceptualization; **Ramesh Chand**: supervision; **Deepti Saxena**: supervision; **Aman Kumar**: writing – original draft.

Conflict of interest

The authors declare that they have no conflict of interest.

References

1. Shrivastav N, Madan J, Pandey R, Shalan AE. Investigations aimed at producing 33% efficient perovskite–silicon tandem solar cells through device simulations. *RSC Advances.* 2021;11(59): 37366–37374.
2. Carrasco J, Illas F, Lopez N, Kotomin EA, Zhukovskii YF, Evarestov RA, Mastrikov Y, Piskunov S, Maier J. First-principles calculations of the atomic and electronic structure of F centers in the bulk and on the (001) surface of $SrTiO_3$. *Physical Review B.* 2006;73: 064106.
3. Noor NA, Mahmood Q, Rashid M, UlHaq B, Laref A, Ahmad SA. Ab-initio study of thermodynamic stability, thermoelectric and optical properties of perovskites $ATiO_3$ (A = Pb, Sn). *Journal of Solid State Chemistry.* 2018;263: 115–122.
4. Mahmood Q, Yaseen M, Haq BU, Laref A, Nazir A. The study of mechanical and thermoelectric behavior of $MgXO_3$ (X = Si, Ge, Sn) for energy applications by DFT. *Chemical Physics.* 2019;524: 106–112.
5. Mahmood Q, Haq BU, Yaseen M, Ramay SM, Ashiq MG, Mahmood A. First-principle study of mechanical, optical and thermoelectric properties of $SnZrO_3$ and $SnHfO_3$ for renewable energy applications. *Solid State Communications.* 2019;292: 17–23.

6. Noor A, Rashid M, Mahmood Q, Haq BU, Naeem MA, Laref A. Optoelectronic pressure dependent study of $MgZrO_3$ oxide and ground state thermoelectric response using Ab-initio calculations. *Opto-Electronics Review.* 2019;27(2): 194–201.
7. Wang D, Ye J, Kako T, Kimura T. Photophysical and photocatalytic properties of $SrTiO_3$ doped with Cr cations on different sites. *Journal of Physical Chemistry B.* 2006;110(32): 15824–15830.
8. Kumar S, Tiwari SC, Gupta A, Verma A, Kumar A. Comprehensive study of $BaAlO_3$ using FP-LMTO and PBE-GGA: Structural, electronic, and optical properties. *Semiconductors.* 2025;59: 495–501.
9. Evans DJ, Williams SR, Searles DJ. On the entropy of relaxing deterministic systems. *Journal of Chemical Physics.* 2011;135(19): 194107.
10. Aguado-Puente P, Junquera J. Ferromagneticlike closure domains in ferroelectric ultrathin films: First-principles simulations. *Physical Review Letters.* 2008;100: 177601.
11. Liu QJ, Zhang NC, Liu FS, Wang HY, Liu ZT. $BaTiO_3$: Energy, geometrical and electronic structure, relationship between optical constant and density from first-principles calculations. *Optical Materials.* 2013;35(12): 2629–2637.
12. Maldonado F, Rivera R, Villamaguan L, Maldonado J. DFT modelling of ethanol on $BaTiO_3$ (001) surface. *Applied Surface Science.* 2018;456: 276–289.
13. Akbar A, Imad K, Zahid A, Fawad K, Iftikhar A. First-principles study of $BiFeO_3$ and $BaTiO_3$ in tetragonal structure. *International Journal of Modern Physics B.* 2019;33(21): 1950231.
14. Xiao CJ, Jin CQ, Wang XH. Crystal structure of dense nanocrystalline $BaTiO_3$ ceramics. *Materials Chemistry and Physics.* 2008;111(2–3): 209–212.
15. Fan Z, Sun K, Wang J. Perovskites for photovoltaics: A combined review of organic–inorganic halide perovskites and ferroelectric oxide perovskites. *Journal of Materials Chemistry A.* 2015;3(37): 18809–18828.
16. Iram N, Sharma R, Ahmad J, Kumar A, Kumar A, Almutairi FN, Alturaifi HA. A DFT Manifestation of the physical, thermodynamic and thermoelectric properties in Sn-based halide perovskites. *Inorganic Chemistry Communications.* 2024;172: 113573.
17. Nechache R, Harnagea C, Li S, Cardenas L, Huang W, Chakrabartty J, Rosei F. Bandgap tuning of multiferroic oxide solar cells. *Nature Photonics.* 2015;9(1): 61–67.
18. Diéguez O, Rabe KM, Vanderbilt D. First-principles study of epitaxial strain in perovskites. *Physical Review B.* 2005;72: 144101.
19. King-Smith RD, Vanderbilt D. First-principles investigation of ferroelectricity in perovskite compounds. *Physical Review B.* 1994;49: 5828–5844.
20. Kumar A, Kumar A, Iram N. First-principles calculations to investigate structural, electronic, mechanical, and optical properties of $SrAlO_3$ compound. *Hybrid Advances.* 2024;6: 100211.
21. Gao H, Cao J, Liu L, Yang Y. Theoretical investigation on the structure and electronic properties of barium titanate. *Journal of Molecular Structure.* 2011;10003(1–3): 75–81.
22. Kumar A, Kumar R, Saxena D, Nautiyal VK, Kumar A, Iram N. Structural, electronic, magnetic and optical properties of $GdCuX_2$ (X = S, Se and Te) compounds. *Optical and Quantum Electronics.* 2024;56: 1742.
23. Kumar A, Kumar A, Jain P, Pundir SK, Singh N. TB-mBJ for doping concentration effects on magneto-optical properties in ZnMn *x* Sn (1-*x*) As 2 spintronics materials. *Optik.* 2024;315: 172039.
24. Kumar A, Gupta H, Kumar A, Kumar A, Sharma SK, Lal B, Iram N. Optoelectronic properties of Sb doped GaAs: DFT investigation. *Indian Journal of Physics.* [Preprint] 2024. Available from: doi.org/10.1007/s12648-024-03273-6
25. Kumar A, Kumar A, Iram N. First-principles calculations to investigate structural, electronic, mechanical and optical properties of $SrAlO_3$ compound. *Hybrid Advances.* 2024;6: 100211.
26. Kumar A, Kumar A, Kumar A, Iram N. Ab-initio study of hybrid perovskites $Cs_2AgGaCl_6$ for solar cells applications. *Hybrid Advances.* 2024;6: 100197.
27. Gautam R, Kumar A, Singh RP. First Principle Investigations on Electronic, Magnetic, Thermodynamic, and Transport Properties of $TlGdX_2$ (X = S, Se, Te). *Acta Physica Polonica A.* 2017;132(4): 1371–1378.
28. Annveer, Gautam R, Kumar A, Kumar A, Gautam YK, Saroj AL, Singh RP. Study of optoelectronic and thermoelectric spectra of $Tl(Nd/Gd)S_2$. *Journal of Materials Science: Materials in Electronics.* 2021;32: 727–744.
29. Bilc DI, Orlando R, Shaltaf R, Rignanese GM, Íñiguez J, Ghosez P. Hybrid exchange-correlation functional for accurate prediction of the electronic and structural properties of ferroelectric oxides. *Physical Review B.* 2008;77: 165107.
30. Blaha P, Schwarz K, Tran F, Laskowski R, Madsen GK, Marks LD. WIEN2k: An APW+lo program for calculating properties of solids. *Journal of Chemical Physics.* 2020;152: 23411–123417.

31. Kumar A, Kumar A, Kumar K, Singh RP, Singh R, Kumar R. The Electronic and Thermodynamic Properties of Ternary Rare Earth Metal Alloys. *East European Journal of Physics.* 2023;1: 109.
32. Wemple SH, DiDomenico M, Camlibel I. Dielectric and optical properties of melt-grown $BaTiO_3$. *Journal of Physics and Chemistry of Solids.* 1968;29(10): 1797–1803.
33. McCabe CJ, Halvorson MA, King KM, Cao X, Kim DS. Interpreting interaction effects in generalized linear models of nonlinear probabilities and counts. *Multivariate Behavioral Research.* 2022;57(2–3): 243–263.
34. Tran F, Blaha P. Accurate band gaps of semiconductors and insulators with a semilocal exchange-correlation potential. *Physical Review Letters.* 2009;102: 226401.
35. Barlidó P, Aull T, Huran AW, Tran F, Marques MAL. Large-scale benchmark of exchange-correlation functionals for electronic band gaps of solids. *Journal of Chemical Theory and Computation.* 2019;15(9): 5069–5079.
36. Momma K, Izumi F. VESTA 3 for visualization of crystal, volumetric and morphology data. *Journal of Applied Crystallography.* 2011;44: 1272–1276.
37. Kumar A, Gupta H, Kumar D, Sharma R, Kumar A, Sharma SK, Singh AP. Study of Structural and Electronic Properties of $CsMgCl_3$ Compound. *East European Journal of Physics.* 2024;1: 355.
38. Annveer, Gautam R, Kumar A, Kumar A, Singh PK, Singh RP. Magneto-optical effects in half metallic ferromagnets: Rare earth thallium tellurides ($TlXTe_2$; X = Tb-Er). *Optik.* 2020;223: 165317.
39. Kumar A, Guatam R, Chand S, Kumar A, Singh RP. First principle electronic, magnetic and thermodynamic characterization of heavy fermion ternary rare earth metal alloys. *Materials Physics and Mechanics.* 2019;42(1): 112–130.